Title
Murine maternal dietary restriction affects neural Humanin expression and cellular profile

Journal
Journal of Neuroscience Research, 98(5)

ISSN
0360-4012

Authors
Baldauf, Claire
Sondhi, Monica
Shin, Bo-Chul
et al.

Publication Date
2020-05-01

DOI
10.1002/jnr.24568

Peer reviewed

HHS Public Access

Author manuscript

J Neurosci Res. Author manuscript; available in PMC 2020 December 16.

Published in final edited form as:

J Neurosci Res. 2020 May ; 98(5): 902–920. doi:10.1002/jnr.24568.

Murine Maternal Dietary Restriction Affects Neural Humanin Expression and Cellular Profile

Claire Baldauf, MD[1], **Monica Sondhi, MD**[1], **Bo-Chul Shin, PhD**[1], **Young Eun Ko, BS**[1], **Xin Ye, MD**[1], **Kuk-Wha Lee, MD, PhD**[2], **Sherin U Devaskar, MD**[1]

[1]Department of Pediatrics, Divisions of Neonatology & Developmental Biology, UCLA Children's Discovery and Innovation Institute, David Geffen School of Medicine at the University of California, Los Angeles, Los Angeles, CA, 90095, U. S. A.

[2]Department of Pediatrics, Division of Endocrinology, Neonatal Research Center of the UCLA Children's Discovery and Innovation Institute, David Geffen School of Medicine at the University of California, Los Angeles, Los Angeles, CA, 90095, U. S. A.

Abstract

To understand the cellular basis for the neurodevelopmental effects of intra-uterine growth restriction (IUGR), we examined global and regional expression of various cell types within murine (*Mus musculus*) fetal brain. Our model employed maternal calorie restriction to 50% daily food intake from gestation day 10-19, producing IUGR offspring. Offspring had smaller head sizes with larger head:body ratios indicating a head sparing IUGR effect. IUGR fetuses at embryonic day 19 (E19) had reduced nestin (progenitors), β-III Tubulin (immature neurons), GFAP (astrocytes), and O4 (oligodendrocytes) cell lineages via immunofluorescence quantification and a 30% reduction in cortical thickness. No difference was found in Bcl-2 or Bax (apoptosis) between controls and IUGR, though qualitatively, doublecortin (migration) and Ki67 (proliferation) immunoreactivity were decreased. In the interest of examining a potential therapeutic peptide, we next investigated novel pro-survival peptide, mouse Humanin (mHN). Ontogeny examination revealed highest mHN expression at E19, diminishing by post-natal day 15 (P15) and nearly absent in adult (3 month). Sub-analysis by sex for mHN expression yielded higher mHN expression among males during fetal life, without significant difference between sexes post-natally. Further, IUGR had a greater increase in cortical mHN in the female versus the male fetus over their respective controls. We conclude that maternal dietary restriction associated IUGR interferes with neural progenitors differentiating into the various cellular components populating the cerebral cortex and reduces cerebral cortical size. mHN expression is developmental stage and sex specific, with IUGR, particularly in the females, adaptively increasing its expression towards mediating a pro-survival approach against nutritional adversity.

Corresponding Author: Sherin U. Devaskar, 10833 Le Conte Avenue, 22-412 MDCC, Los Angeles, CA 90095, Tel: 310-825-5095, Fax: 310-206-4584, sdevaskar@mednet.ucla.edu.

Author Contributions: Authors C.B., B.S. and S.U.D. had full access to the data in the study and take responsibility for the integrity of the data and accuracy of the data analysis. *Conceptualization*, C.B., M.S. and S.U.D.; *Methodology*, C.B., K.W.L., B.S. and S.U.D.; *Investigation*, C.B., M.S., B.S., X.Y. and Y.K.; *Formal Analysis*, C.B., M.S., X.Y. and B.S.; *Resources*, C.B., B.S. and S.U.D.; *Writing - Original Draft*, C.B.; *Writing - Review & Editing*, and revisions C.B. and S.U.D.; *Visualization*, C.B. and B.S.; *Supervision*, B.S. and S.U.D.; *Funding Acquisition*, S.U.D. and C.B.

Conflicts of Interest: The authors declare no competing financial interests.

Graphical Abstract

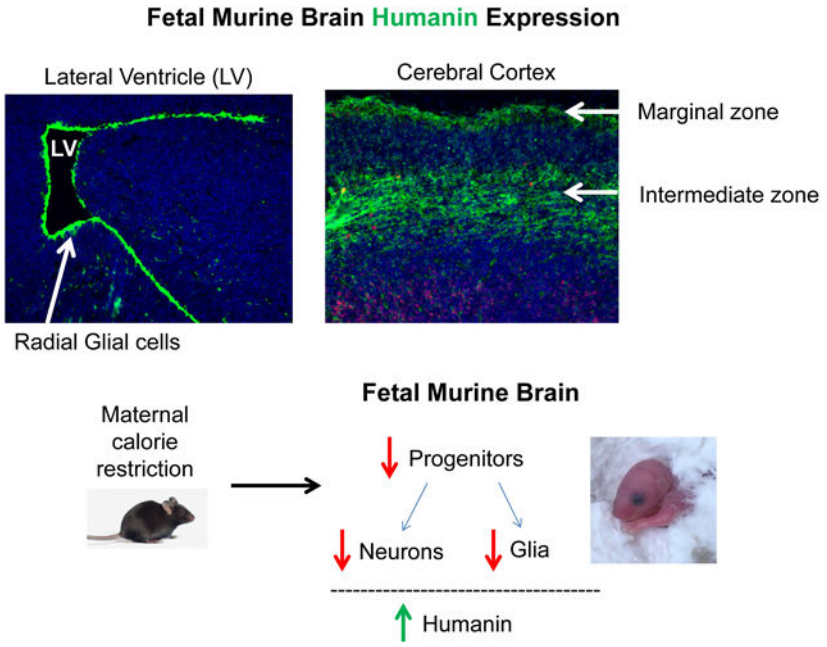

Keywords

Intra-uterine growth restriction; Humanin; neurodevelopment; nutrient restriction; fetal brain

RRIDs:

AB_532250; AB_1616567; AB_2313773; AB_1619688; AB_772206; AB_631729; AB_2336177; SCR_014246; AB_10950489; AB_477629; AB_561053; AB_650336; AB_2286684; AB_793998; AB_477662; AB_2313584; AB_2340432; AB_2340375; AB_305670; AB_10695870; AB_443209; AB_732011; SCR_002368; SCR_002140; SCR_013673; SCR_002798

Introduction

Intra-uterine growth restriction (IUGR) refers to an infant who does not reach full growth potential due to a pathologic insult during intra-uterine life and affects up to 10% of pregnancies (Longo et al., 2013; Resnik, 2002; Vandenbosche & Kirchner, 1998). IUGR is a world-wide problem and in the U.S. pre-eclampsia and hypertension are prevailing causes (Vandenbosche & Kirchner, 1998). IUGR is a major risk factor for adverse neurodevelopmental outcomes including intellectual disability and cerebral palsy (Jacobsson et al., 2008; Jarvis et al., 2003; Leitner et al., 2007; Pryor, Silva, & Brooke, 1995; Robertson, Etches, & Kyle, 1990; Smedler, Faxelius, Bremme, & Lagerstrom, 1992; Strauss, 2000). In addition, growth restricted infants are at increased risk of emotional and behavioral disorders in childhood such as attention deficit, hyperactivity, and depression (Dahl et al., 2006; Raikkonen et al., 2008; Zubrick et al., 2000).

While the most common cause of IUGR in humans is related to placental disease, the end result experienced by the developing embryo is ischemia and a global restriction in the availability of nutrients. Multiple animal models have been developed to mimic this condition, including our previously and widely examined maternal calorie restriction mouse or rat model. Using this model, where 50% caloric restriction is brought about from mid-through late gestation, the fetuses are noted to be intra-uterine growth restricted (IUGR). This phenotype is secondary to a reduction in utero-placental blood flow (Ganguly, Touma, Thamotharan, De Vivo, & Devaskar, 2016; Garris, 1984; Giambrone & Warrington, 2018; Hernandez-Andrade et al., 2014) with resulting ischemia, along with a diminution in trans-placental nutrient supply (Ganguly, Collis, & Devaskar, 2012; Giambrone & Warrington, 2018). Our previous investigations have revealed that the long term effect of such IUGR consists of various chronic disorders (Garg et al., 2013; Garg et al., 2012), including neuropsychological changes that last into adult life (Tomi, Zhao, Thamotharan, Shin, & Devaskar, 2013). However, not much is known about the impact of such diminished trans-placental nutritional availability on fetal brain development, particularly the cellular profile. Based on this major gap in knowledge, we hypothesized that maternal caloric restriction will be detrimental to fetal brain development resulting in a disorganized cellular profile, thereby requiring future investigation into potential therapeutic options.

To this end, the human Humanin (HN) peptide, first discovered in 2001 using a cDNA death trap screen in a preserved region of an Alzheimer's disease brain (Hashimoto et al., 2001), may provide such an option. The HN open reading frame is greater than 99% identical to the mitochondrial 16S ribosomal RNA (gene name: MTRNR2) (Capt, Passamonti, & Breton, 2016; Hashimoto et al., 2001; Maximov, Martynenko, Hunsmann, & Tarantul, 2002). However, sequences with strong resemblance to the mitochondrial open reading frame are present in the nuclear DNA (Tajima et al., 2002). The translation site of HN is not yet clear, but HN is secreted from its site of origin as evidenced by its presence in plasma, CSF, and seminal fluid (Chin et al., 2013; Moretti et al., 2010; Widmer et al., 2013). Adult HN plasma concentrations appear to decrease with age in both humans and mice (Muzumdar et al., 2009), with upregulation in certain disease states associated with oxidative or metabolic stress. HN has been shown to be increased in the plasma of women with pre-eclampsia compared to those with uncomplicated pregnancies (Nikolakopoulos et al., 2018), is higher in the skeletal muscle fibers of patients with mitochondrial encephalomyopathy with lactic acidosis and stroke-like episodes (MELAS) than for controls (Kariya, Hirano, Furiya, Sugie, & Ueno, 2005), and upregulated in murine cardiac myocytes subsequent to myocardial infarction with reperfusion injury (Muzumdar et al., 2010).

HN has been shown to be neuroprotective in several models of adult neurologic disease. It is most extensively studied in murine models of Alzheimer's disease, where exogenous administration has been shown to inhibit Aβ neurotoxicity and improve functional outcomes (Chai et al., 2014). Similar findings have been seen with adult models of stroke and amyotrophic lateral sclerosis (Matsuoka, Hashimoto, Aiso, & Nishimoto, 2006; Xu, Chua, Gao, Hamdy, & Chua, 2006). HN's protective properties have also been demonstrated in cell culture using models of hypoxia, toxins, and conditions of oxidative stress (Cui et al., 2017; Men, Zhang, Yang, & Gao, 2012; Sreekumar et al., 2016; Zhao, Wang, Li, Zhao, & Zhang, 2014). A common theme in these studies is promotion of cell survival under stressful

conditions consisting of an energy deficit, and cellular degeneration/apoptosis. However, not much is known about HN's role in embryonic brain development nor in response to maternal caloric restriction. Therefore, prior to any consideration as a potential therapeutic target, it is important to determine whether HN is expressed in fetal brain, and if so at what developmental stage. We therefore examined mouse Humanin (mHN) (mus musculus) expression at differing developmental time points. We subsequently compared its expression in control versus maternal caloric restriction associated intra-uterine growth restricted (IUGR) fetal brains. We asked whether mHN would be upregulated in response to the fetal stressor of energy deficit. Our studies here employed our well characterized maternal caloric restriction mouse model (Ganguly et al., 2012; Ganguly et al., 2016) to initially examine the effect on the embryonic cellular profile, including cellular processes (proliferation and apoptosis). These investigations were followed by the ontogeny of mHN in embryonic and postnatal control brains, cell-specific localization in embryonic brain, and subsequently in the IUGR embryonic brains to decipher if this novel pro-survival peptide had the potential for future exploration as a therapeutic target.

Methods

Murine Animal Model

Wild Type C57/BL6 mice were purchased from the UCLA Division of Laboratory Animal Medicine (DLAM; obtained from The Jackson Lab, Bar Harbor, ME). The mice were maintained in 12:12-h light-dark cycles and care/treatment provided according to UCLA Animal Research Committee's (ARC) approved protocol in accordance with the guidelines set by the National Institutes of Health and the Guide for the Care and Use of Laboratory Animals. Following mating, detection of a vaginal plug was designated as gestation day 1. Fetal IUGR was induced by providing 50% of daily calories (1.875g mouse chow/day) to pregnant dams from gestation day 10-19 (from mid to late gestation). Standard mouse chow used was type NIH-31 modified 7013 diet (carbohydrate 45g%/59kcal%, fat 6.2g%/ 18%kcal, and protein 18g%/23kcal%; Teklad Inc., Madison, WI). Chow was weighed daily for the IUGR group to provide the appropriate amount of chow. Control animals received ad libitum access to chow. Both groups had ad libitum access to water. Fetuses were delivered by hysterotomy at E19 following administration of isoflurane via inhalation. After weighing the placenta and whole fetus, fetal heads were also weighed.

Immunohistochemical Analysis

Pregnant dams at embryonic (E) day 10, 15 and 19, post-natal day 15 (P15) and 3 month old adult mice were perfused with 4% paraformaldehyde. Fixed fetal brain tissues were washed in PBS for 30 minutes, five times, then placed in 20% sucrose in 0.1 M sodium phosphate buffer, pH 7.4, containing 0.02% sodium azide, and embedded in O.C.T. compound (VWR Scientific, Cat# 25608-930). Specimens were frozen in liquid nitrogen and then 10-μm sections mounted onto glass slides using a cryostat (Leica Microsystems, CM 1850, Nussloch, Germany). Immunofluorescence staining was initiated by blocking slides in 5% normal donkey serum with 1% gelatin containing 0.2% Triton X-100 in PBS for 1 hour (Shin et al., 1996; Tserentsoodol, Shin, Koyama, Suzuki, & Takata, 1999). Blocking was followed by incubation with primary antibody. All primary antibodies were incubated for 1

hour at room temperature plus overnight at 4°C. After washing slides three times for 10 min each, fluorescent conjugated secondary antibodies were used as applicable by host species. All primary and secondary antibody details can be found in Table 1. Slides were examined by a Nikon Eclipse E600 microscope (Nikon, Melville, NY) equipped with a cooled, charge-coupled device camera CoolSNAP HQ Monochrome (Roper Scientific, Tuscon, AZ, www.photometrics.com). Imaging and semi-quantification of fluorescence of the above cellular markers was performed with MetaMorph Microscopy Automation and Image Analysis Software (www.moleculardevices.com, RRID: SCR_002368). Two regions, the subventricular zone (SVZ) and the cerebral cortex (Cx) were examined. Three consecutive slides were selected, and the right and left side of each slide was measured (six measurements). Values from the three slides in each region were averaged to constitute an n=1 for each region (SVZ and Cx). Quantification of each group was performed and reported as a relative percent of the respective control group. Confocal microscopy was performed with the Leica TCS SP-8 microscope (www.leica-microsystems.com, RRID: SCR_002140) and videos created using Leica Application Suite X software (www.leica-microsystems.com, RRID: SCR_013673).

TUNEL assay for apoptosis

Frozen sections (10 μm) were processed using a TUNEL detection kit as described by the manufacturer (Click iT TUNEL Alexa FluorTM 594 Imaging Assay, Molecular Probes, Eugene, OR). Briefly, tissue sections were washed with PBS and incubated at room temperature for 1 hour with a blocking solution including 3% BSA-0.25% Triton X-100 in PBS. Some sections were treated by DNase I for standard breaks in the DNA as a positive control. Subsequently, all sections were washed with distilled water, incubated for 3 hours at 37°C in the reaction cocktails including TdT (terminal deoxynucleotidyl transferase) prepared from kit. Sections as a negative control were incubated in reaction cocktails with the absence of TdT. Continuously, all sections including a negative and a positive control were incubated for 30 min at room temperature in the Click-iT reaction buffer prepared from the kit. After washing twice with 3% BSA in PBS, all sections were incubated in DAPI (4′, 6-diamino-2-phenylindole dihydrochloride) for 15 min at room temperature, washed twice with PBS and mounted. All brain sections were reviewed using a Nikon E-600 fluorescence microscope.

Cortical Thickness Measurement

Haematoxylin and eosin (H&E) staining was performed on the fetal brain sections of IUGR and control E19 brains as prepared for immunohistochemistry (described above). Using the above MetaMorph software, cortical thickness was measured from the edge of the lateral ventricle through the marginal zone in a perpendicular orientation to the cortical layers. The intermediate zone was measured in the same fashion taking care to measure the distance between the cortical plate and subventricular zone layers. Care was taken that the brain region measured was the same in all specimens.

Western Blot Analysis

Brains from E19, P15, and 3 month old mice were taken after skull removal. Whole brains, were collected in addition to microscopically separated subventicular zone (SVZ) and

cerebral cortex (Cx). Brain regions were separated in a glass petri dish placed on ice employing established anatomical landmarks (Schambra, 2008). Brain tissues were snap-frozen in liquid nitrogen, and then powdered on dry ice. A mixture of RIPA lysis buffer containing protease and phosphatase inhibitors (ThermoFisher Scientific, Cat#s 89901, 88669) and 1 mM PMSF was next added, and the samples were then homogenized using a high-speed homogenizer prior to sonication. Homogenates were centrifuged at 10,000 rpm at 4°C for 10 min and the supernatant collected for protein concentration estimation by the Bio-Rad protein assay kit (Bio-Rad Laboratories, Cat# 500-0006). Samples were then stored at −80°C until further analyses.

Whole brains and brain sub-fraction (SVZ or Cx) lysate homogenates were boiled in a water bath for six minutes and loaded onto a 4-12% Bis-Tris gel (Life Technologies, Cat# NP0335BOX) and subjected to SDS-PAGE. Separated proteins were transferred to a PVDF membrane (Bio-Rad Laboratories, Cat# 1620174) and the membranes blocked in 5% bovine serum albumin in phosphate-buffered saline containing 0.1% Tween 20 (PBST) for 1 hour. Membranes were incubated with antibody mixed in 5% bovine serum albumin in PBST. Various blocking reagents (bovine serum albumin, Seablock, non-fat milk solution) were pre-tested towards optimization, of which 5% bovine serum albumin was noted to be most effective in the case of mHN detection. Primary antibodies were incubated for 1 hour at room temperature with the exception of α-Humanin which was incubated at 4°C overnight in addition to 1 hour at room temperature. The incubation period for mHN was optimized based on prior incubation timed experiments conducted over various durations. Membranes were washed six times for 5 minutes each, before incubation with secondary antibody. Details of primary and secondary antibodies used can be found in Table 1. Membranes were then washed three times for 10 minutes each. Bands were detected by enhanced chemiluminescence (Thermo Fisher Scientific, Cat# 32132) and protein density quantified using Image Quant software (GE Healthcare, RRID: SCR_014246). Optical density was adjusted for loading variability using an internal control. Depending on size of the protein being quantified, internal control was one of: α-β-actin, α-Vinculin, or α-GAPDH. All were incubated for 30 minutes each at room temperature. All protein densities are reported as a ratio of protein/loading control. Co-immunoprecipitation of mHN and Notch-1 proteins was performed using Protein G coupled magnetic beads (Life Technologies, Cat# 10007D). E19 whole brain lysate was incubated with anti-HN or anti-Notch-1 antibody, after which the eluent was subjected to western blot analysis and imaged with chemiluminescence (antibodies and imaging as described above).

Antibody Characterization

Humanin antibody: HN and mHN have similar expected molecular weight (MW) of approximately 3-6kD. Humanin protein is known to make dimers, trimers, and oligomers that are necessary for its function in vivo (Arakawa, Niikura, Tajima, & Kita, 2006; Terashita et al., 2003). Tajima et al showed binding to endogenous mHN with a 3-6kD band seen in testis and colon of 3 week old mice. These bands disappeared with antibody pre-adsorption (Tajima et al., 2002). A western blot (WB) band below 10kD (specific size not mentioned) using cells isolated from a rat model was published in 2018 (Gong et al., 2018). Additionally, in this study, binding of antibody to endogenous rat HN (rHN) and synthetic

HN peptide at the lysosomal surface of rat cells blocked normal downstream autophagy activity indicating binding of the antibody to its expected target. rHN has been found to be expressed via WB in the following rat tissues: skeletal muscle, liver, epididymal fat, hypothalamus as well as via reverse transcription polymerase chain reaction (RT PCR) in the cortex, hippocampus, cerebellum, kidney, liver, lung, skeletal muscle, spleen, testis and uterus (Muzumdar et al., 2009). HN and mHN have also been found in plasma using enzyme-linked immunosorbent assay (ELISA) in both human subjects and mice respectively (C. Lee et al., 2014). In our lab, we found mHN in whole brain lysates immunoprecipitated with anti-HN antibody showing a band at both 6 and 14 kD, 6 kD being the reported molecular weight, and the 14 kD being an oligodimer.

The remaining primary antibodies discussed below were used as tissue markers or have extensive published data supporting their validity. Tissue marker staining appeared in the expected pattern of cellular morphology and those western blotted demonstrated band sizes of expected molecular weight as found in previous publications: α-Notch-1 (Kostyszyn, Cowburn, Seiger, Kj, & Sundstrom, 2001), α-Sox-2 (S. Wang et al., 2010), α-nestin (Frederiksen & McKay, 1988; Yoshimatsu et al., 2006), α-Vimentin (Lavado & Oliver, 2011; Middeldorp et al., 2010), α-GFAP (H. S. Lee, Han, Lee, Park, & Kim, 2010; Middeldorp et al., 2010), α- β-III Tubulin (H. S. Lee et al., 2010; Menezes & Luskin, 1994), α-O4 (Sommer & Schachner, 1981; Windrem et al., 2004), α-Bax (Wnuk, Rzemieniec, Litwa, Lason, & Kajta, 2018; Xiao & Zhang, 2008), α-Bcl-2 (Li, Chen, & Zhou, 2013; Xiao & Zhang, 2008), α-Doublecortin (Corbo et al., 2002; Mizuguchi, Qin, Yamada, Ikeda, & Takashima, 1999), α-Ki67 (Tolcos et al., 2015). Further details of primary antibodies can be found in Table 1.

Sex as a Biological Variable

Inter-sex variability was examined and reported in the examination of whole brain, SVZ and Cx mHN expression over developmental time points E19, P15, and adult, as well as between E19 IUGR and controls (via western blot analysis). A total of 37 males and 37 females were included in the study. The remaining data analyses, again denoted in the results and figure legends, were not sub-analyzed as animals were not sexed prior to obtaining samples.

Genotyping for Sex Determination

Genetic sex determination of E19 embryos was performed on extracted tail DNA using PCR primers that amplify DNA fragments of either the X-chromosomal Xlr gene (X-linked lymphocyte-regulated complex) or the Y-chromosomal Sly gene (Sycp3-like Y-linked) (McFarlane, Truong, Palmer, & Wilhelm, 2013). The PCR conditions consisted of denaturation at 95°C for 2 minutes, followed by 35 cycles of denaturation at 95°C for 30 seconds, annealing at 58°C for 30 seconds, and extension at 72°C for 30 seconds. Finally, extension at 72°C for 5 minutes was done. Sex at P15 and adult stages was determined by visualization of the external genitalia.

Statistical Analysis

Data are presented as mean ± standard error of the mean (SEM) or as mean ± standard deviation (SD; towards optimizing graphical presentation). GraphPad Prism software

(www.graphpad.com, RRID: SCR_002798) or StatView Version 5.0 (SAS institute Inc, Cary, NC, SCR_017411) were used for graphical representation and statistical analyses. A power analysis was performed that revealed an n=8/group to obtain a power of 0.80 with α=0.05 for quantitative experiments (e.g. western blots). Two tailed Student t-test was employed for comparing each animal group against the respective control (two groups). One-way ANOVA was used for comparing three groups to one another with Tukey post-hoc analysis performed within the statistical software. A *P*-value <0.05 was considered significant. Outliers from each experiment were included in the results, and normalcy of distribution tested to employ parametric tests. Test for equal variance was performed for each calculation and assumed where non-significant. For qualitative analysis as in immunolocalization studies, replication of experiments with an n=2 arising from different litters was performed to confirm the observations.

Results

Fetal Weight and Head Sizes in IUGR Animals

There were significant differences found in biometrics between fetal IUGR and control (CON) pups at E19 (CON n=69, IUGR n=48). Using a two-tailed Student t-test, we found IUGR animals were 42% smaller in total body weight (t_{77} = 13.26; P<0.001), with head weights 36% lower than controls (t_{90} = 12.5; P<0.001). The ratio of head to body weight was 14% higher in IUGR animals (t_{77} = −5.43; P<0.001). These observed patterns indicate a brain sparing effect of this IUGR model.

Cellular profile changes in the IUGR fetal brain

We first examined E19 IUGR versus CON brains via immunofluorescence to evaluate localization and location specific quantification of cell type specific marker expression. We found a significant reduction in Nestin (progenitors) expression in the SVZ and cerebral cortex (Cx) of the IUGR brain (Fig. 1 a-d, q). Examination of specific cell type β-III Tubulin (immature neurons) (Fig. 1 e-h, r), GFAP (astrocytes) (Fig. 1 i-l, s), and O4 (immature, mature, and pre-oligodendrocytes) (Fig. 1 m-p, t) all revealed a reduction in SVZ and Cx expression in the IUGR brain compared to CON.

Since the expression and numbers of progenitor neural cells, oligodendrocytes, astrocytes, and neurons were altered in the IUGR brain, murine E19 whole brains, separated SVZ and Cx region lysates were subjected to Western blot analysis to quantify IUGR versus control expression of nestin (progenitors), GFAP (astrocytes), and β-III Tubulin (immature neurons) (Fig. 2). In the whole brain, a decrease in GFAP alone was evident in IUGR versus CON (by 34%, P=0.018; Supplemental Figure 1), with no change in nestin and β-III Tubulin. Among IUGR males (Fig. 2b), nestin expression in SVZ and GFAP expression in the Cx were significantly lower than controls (by 75.3%, P=0.0493 and 70.1%, P=0.018 respectively). Female animals (Fig. 2c) and comparisons of β-III Tubulin demonstrated no significant differences.

Cellular Process Changes in IUGR Fetal Brain

We examined doublecortin immunoreactivity as a marker of neural cell migration and observed a qualitative reduction in the E19 IUGR versus CON brains (Figure 3 a-d). Ki67 immunoreactivity that reflects cell proliferation was noted to be qualitatively reduced in the SVZ region of the IUGR versus CON fetal brain (Figure 3 e-h), although no difference was observed in the TUNEL assay that assessed cellular apoptosis (Supplemental Figure 2). Since TUNEL positive cells were low in both CON and IUGR brain sections, we further assessed Bcl-2 (anti-apoptosis) and Bax (pro-apoptosis) protein concentrations in whole brains (pooled male and female samples) by western blot analysis as additional markers for cellular apoptosis. While trends toward an increase were seen, no significant differences were observed using two tailed Student t-test (Bcl-2 mean ± SEM: CON = 100.3±22.73, IUGR = 138.6 ± 20.6; [t_{13}=1.25; n=7; CON, n=8 IUGR; P=0.23]; Bax mean ± SEM: CON = 100 ± 11.25, IUGR=123.4 ± 25.34; [t_{14}= 0.84; n= 8/group P=0.41]).

Cortical Thickness

Given the changes in cellular profile between IUGR and control brains at E19, we measured the cerebral cortex thickness to determine whether it is also affected by fetal growth restriction. We found a 29.5% reduction in cortical thickness in the IUGR brain when compared to control (Fig. 4) (P=0.031). Given the presence of mHN in the intermediate zone, we also measured the thickness of this cortical layer. The IUGR intermediate zone was 71% smaller than CON (Fig. 4) (P=0.0007). The CON intermediate zone comprised 43% of total cortical thickness while in IUGR this layer comprised only 30% of total thickness (P=0.004).

mHN exhibits a specific localization pattern and ontogeny in murine brain

Whether mHN is expressed in the cortex or ventricular/subventricular regions has not been reported. Using immunofluorescence, we examined C57/BL6 mice for endogenous mHN expression at four developmental time points, n=2 animals/group: embryonic day 19 (E19), 15, and 10, and the 3-month old adult brain. At E10, the cortex contains only two zones, ventricular zone and pre-plate (Kondo, Al-Hasani, Hoerder-Suabedissen, Wang, & Molnar, 2015). We found mHN expressed throughout both zones at this time point (Fig. 5 a-c). At E15, we found mHN present in the cerebral cortex, with expression strongest in the marginal and intermediate zones. We also found strong mHN expression around the lateral ventricle (Fig. 5 d-f). At E19 mHN's cortical expression pattern is very similar to that at E15 with expression in the same regions (Fig. 5 g-i). Very minimal mHN immunoreactivity was found in the adult cortex and subventricular regions (Fig. 5 j-l). In order to examine where in the periventricular cells mHN expresses, confocal immunofluorescence microscopy was done on an E19 brain which demonstrated expression at the apical surface of the cells lining the lateral ventricle (Supplemental Video 1).

We then quantified mHN expression via western blot analysis using lysate of whole brain (Supplemental figure 1), as well as separated Cx and SVZ brain regions (Fig. 6) of mice at E19, post-natal day 15 (P15) and 3-month old adult developmental time points. In samples separated by brain region, we found that males had significant differences in mHN expression between all developmental time points, where females did not. Comparing males

at E19 vs P15, there was 40% less mHN at P15 than E19 in both Cx and SVZ regions (both P=0.004). By adulthood for males, there was 83.3% (P<0.001) and 78.7% (P<0.001) less mHN than at E19 in the Cx and SVZ regions respectively. Compared to P15, adult levels of mHN were only 28% (P=0.003) and 35.9% (P=0.005) of P15 levels in the Cx and SVZ respectively. Females showed no significant differences in mHN expression between developmental time points in either the Cx or SVZ. Analysis of results comparing by sex demonstrated a difference only at the E19 time point with males having higher mHN expression in both the Cx (45.6% higher, P=0.001) and SVZ (44.6% higher, P=0.013; n=4/group), when compared to females. Evaluation using whole brain lysates (Supplemental figure 1) showed mHN was also highest during fetal life, with levels at E19 73% greater (P<0.001) than at P15 and 82% greater (P<0.0005) than in adulthood (Supplemental figure 1, d). Sub-analysis of this data by sex showed no difference between males and females at any time point (Supplemental figure 1, e).

Humanin subcellular localization and expression in the context of known periventricular developmental markers

Our findings described above suggest that mHN could be expressed in neural progenitor cells at E19, thus we set out to determine whether mHN demonstrates an expression pattern akin to known developmental markers found in the ventricular region. Using dual immunostaining, we first examined mHN and Vimentin in the E19 murine brain (Fig. 7 a-d). Vimentin is a marker for cells of neuroepithelial and mesenchymal origin (Howard, Chen, & Zecevic, 2006; Zecevic, 2004) and a cytoskeletal marker of several neural cell types including radial glial cells (RGCs). Vimentin was expressed in the choroid plexus, neural progenitor cells surrounding the lateral ventricle (LV), and extended radially from the ventricle (Fig. 7b) (n=2 animals). mHN was expressed in the same cells (Fig. 7c), suggesting that mHN is expressed in neural progenitors and cells surrounding the lateral ventricle (Fig. 7a). We next examined Notch-1 and mHN expression (Fig. 7 e-h) (n=2 animals/group). Notch-1 is a transmembrane protein integral to cell fate determination and helps maintain a pool of progenitors (Artavanis-Tsakonas & Muskavitch, 2010; Artavanis-Tsakonas, Rand, & Lake, 1999). We found Notch-1 expression throughout the ventricular zone (Fig. 7f). Notch-1 and mHN initially appeared to co-localize (Fig. 7g), however upon closer examination by confocal microscopy, they did not (Supplemental Video 2). We also performed co-immunoprecipitation analysis of mHN and Notch-1 and found no evidence of direct protein-protein interaction (data not shown). We next looked at nestin, an intermediate filament protein expressed in progenitor cells during the early stages of CNS development. We found nestin positive neural progenitor cells throughout the ventricular and subventricular zones (Fig. 7j) (n=2 animals/group). We could see that mHN was expressed in many of the same periventricular cells as nestin, but did not appear to co-localize within these cells (Fig. 7i, k). A larger image of nestin staining in the ventricular zone and within neural progenitor cells with mHN can be seen in Supplemental Figure 3. Lastly, we examined Sox-2 expression (Fig. 7 m-p) (n=2 animals/group). Sox-2 is a transcription factor that initiates neural induction and maintains neural progenitor stem cell properties (Tomioka et al., 2002). We found Sox-2 expressed in cells surrounding the lateral ventricle with strong expression extending outward into the ventricular zone (Fig. 7n). There was no co-

localization of mHN and Sox-2 despite their dual presence in progenitor cells lining the LV (Fig. 7o), suggesting that mHN may not be expressed in the nucleus of these cells.

mHN expression in fetal IUGR brain

Initially using Western blot analysis, E19 combined male and female whole brain lysates, IUGR brain was observed to exhibit 77% more mHN than controls (P=0.011; Supplemental Figure 1). Next, using region-specific Cx and SVZ E19 fetal brain lysates, the expression of mHN was further compared in IUGR versus CON via western blotting (Fig. 8a). Results were also sub-analyzed by sex. Due to the presence of two distinct bands at 6kD and 14kD, both bands were quantified and demonstrated similar expression values (Fig. 8b). Utilizing a two-tailed Student t-test, we found that female IUGR Cx had higher mHN than CON, with both 6kD (6.6-fold increase) and 14kD (2.4-fold increase) bands showing significance (P=0.0003 and P=0.001 respectively). This increase achieved in the female IUGR Cx was no different from that present in the male CON Cx. Comparisons between IUGR and CON male and female SVZ were non-significant. However, mHN amount present in the female IUGR SVZ was 48% lower than the male CON SVZ (P=0.036). We next used immunofluorescence to visualize CON and IUGR brain at E19. We found a similar expression pattern in both groups with mHN localized to the periventricular cells, intermediate zone, and marginal zone of the SVZ and Cx (Fig 8c).

Discussion

We observed significant changes in fetal brain cellular profile and processes in response to maternal caloric restriction induced IUGR. These changes consisted of a reduction in neural progenitor cells in the SVZ with an overall reduction in cortical neuronal, glial and oligodendrocytic cellular elements, in conjunction with reduced cortical thickness. In addition, a reduction in cellular proliferation and neural migration was qualitatively evident in the absence of any quantitative changes in apoptosis. Despite the observed IUGR “brain-sparing” effect observed grossly, there were distinct cellular aberrations in IUGR brain. In the face of these key changes, mHN, a pro-survival peptide, whose brain expression peaks during fetal life, increased in the IUGR brain in a sex and location specific manner. Further investigation shows mHN localizing in periventricular cells alongside nestin, Notch-1 and Vimentin. These cells are important developmentally for neural cell migration, thus it is quite possible that mHN plays an important compensatory role towards pro-survival in the presence of reduced progenitor proliferation and neural cell migration in the IUGR embryonic brain.

The regional decreases found in IUGR brain expression of nestin, β-III Tubulin, GFAP, and O4 demonstrate an abnormal cellular profile that fits with previous findings describing reduced cell numbers within IUGR brain as well as reduced myelin content in response to utero-placental insufficiency (Chase, Welch, Dabiere, Vasan, & Butterfield, 1972; Samuelsen et al., 2007). Our western blot data in the IUGR brain showed a reduction in GFAP expression within the male Cx and nestin expression in the male SVZ consistent with the immunofluorescence results; however, the β-III Tubulin, and the remaining GFAP and nestin comparisons were not significantly different. We suspect that measurements in brain

lysates were reliant and influenced by changes in other protein marker expressing cells inhabiting an anatomical region or alternatively, that due to a lesser sensitivity of western blotting there was difficulty in detecting small differences that are tightly region specific and thus seen best by immunolocalization studies. Thus, the Western blot which measures proteins within the context of being 3-dimensional, complements the ability of immunofluorescence to spatially and cell-specifically localize proteins, even if unidimensional. We speculate that the regional reduction in all cell types within IUGR brain seen on immunofluorescence is a result of an arrest in neural precursors' proliferation and/or differentiation which may culminate in smaller cerebral cortices. This speculation was supported by a qualitative reduction in Ki67 immunoreactive cells, a marker of proliferation, and a reduction in doublecortin immunoreactivity, a marker of cell migration. The smaller intermediate zone size within IUGR cortex (both as an absolute value and as a percent of total cortical thickness) suggests IUGR results in a disturbance of the cortical lamination process during development. Developmental disruption has been hypothesized to account for the lower overall brain sizes seen in 3D MRI studies of preterm human IUGR neonates (Padilla et al., 2011; Tolsa et al., 2004). One of the limitations of our study is that the specific cell types that experienced an arrest in proliferation or migration were not deciphered, being beyond the scope of the present study. Such studies in the future will help unravel the affected cellular profile in IUGR brains.

Synthetic HN has been studied extensively as an exogenous agent both in vitro and in vivo to protect against cellular damage and pathological disease states. Less studied however, is the endogenous expression and function of HN. Our findings represent the first describing mHN in murine fetal brain. The ontogeny of mHN we report, with highest expression during fetal life that wanes over time, is consistent with human data from others that circulating HN decreases with age (Muzumdar et al., 2009). Muzumdar et al have also demonstrated that HN expression in rats changes in different tissues at differing ages (Muzumdar et al., 2009), supportive of a disconnect between the developmental timing of peak HN expression in other tissues from that of the brain.

We speculated that embryonic brain outcomes mirror others' findings in adult brain of mHN upregulation after neurologic injury (Chin et al., 2013; Gottardo et al., 2014; Hashimoto et al., 2001). A limitation of having a restricted sample size for sex-specific determinations exists, yet sex-specific differences emerged. We observed males expressing higher amounts of mHN at E19 compared to females. This finding of higher mHN in male fetal brains suggests a higher requirement for mHN expression to maintain normalcy in male versus female neurodevelopment. The female IUGR brain had upregulated mHN in the Cx region, where males did not show a difference in either brain region. This lack of a comparable increase in mHN in males may relate to maximal basal HN expression. These sex-specific changes in the IUGR suggest that the female brain can mount an adaptive response by increasing the expression of pro-survival mHN, while in contrast such an adaptive capability may be lacking in the male IUGR brain. It is possible this difference contributes to the observed incidence of neurodevelopmental consequences being higher in males versus females (Hanamsagar & Bilbo, 2016; Schwarz & Bilbo, 2012; Schwarz, Sholar, & Bilbo, 2012).

mHN expression in the stem cell rich E10 brain and within neural progenitor cells throughout gestation suggests function related to neural proliferation and/or differentiation. We found mHN present within the same periventricular cells positive for nestin, Notch-1 and Vimentin, all markers of neural progenitors such as radial glia. Additional radial glial markers such as GLAST/BLBP were not examined which could pose a relative limitation. Pathways identified for HN by ingenuity pathway analysis of SY5Y cells (a neuroblastoma cell line) point to the Stat-3 and ERK 1/2 pathways (Kim et al., 2016), both of which have known roles in fetal brain development, specifically with respect to neural stem cells (Imamura, Pages, Pouyssegur, Endo, & Takishima, 2010; Sherry, Reeves, Wu, & Cochran, 2009; T. Wang et al., 2015). In addition, the two known receptors for HN, the "trimeric Humanin receptor" and FPRL-1 (formyl peptide receptor like-1) activate the STAT-3 and ERK ½ pathways respectively (Hashimoto, Kurita, Aiso, Nishimoto, & Matsuoka, 2009; Ying et al., 2004). Utilizing a knock-out or transgenic mouse model will be an important next step in mechanistically examining the function of mHN during brain development. It would be interesting as well to examine a knock down model of mHN for potential increases in apoptosis/reduced proliferation suggesting a neuroprotective and perhaps a preventative role during development.

We found sex-specific differences in mHN expression (higher in males) via western blot during fetal life (E19), but not in older animals. The developmental regulation of mHN is not yet well delineated, but there is evidence that mHN is regulated by the growth hormone-IGF-1 axis (C. Lee et al., 2014). Whether this axis or other regulatory pathways have a role in fetal brain mHN expression needs future investigation. We noted in our mHN western blots an expected 6kD band (based upon mHN's expected peptide size) as well as an approximately 14kD band that appeared to closely mimic changes observed with the 6kD band. Given these two bands are visually and statistically consistent with each other, we investigated the 14kD band further to note that this band may represent a mHN oligomer rather than a post-translational modification. Previous studies have found that HN dimerizes and oligomerizes with itself (Arakawa et al., 2006), and furthermore this activity is essential for its neuroprotective effects (Terashita et al., 2003).

Taken together, our data demonstrating abnormal cellular profile, smaller cerebral cortex, and relative microcephaly in the IUGR condition begin to uncover some of the cellular aberrancies that occur due to nutrient deficiency at a critical period of brain development. Nutrient insufficiency encountered as a contributing factor even in human IUGR may underlie the neurodevelopmental delays observed subsequently during infancy and childhood. While mHN within neural progenitors may play an important adaptive role locally within the developing brain, future studies targeting exogenous administration of HN to either the pregnant mother or directly to the fetal brain, may hold some promise and needs to be rigorously investigated.

Conclusions

We conclude that mHN exhibits a specific localization pattern and ontogeny in fetal murine brain. In addition, sex-specific differences in innate fetal brain mHN expression are seen. The ability to adapt to nutrient insufficiency by increasing region specific mHN expression

are more robust in the female than male fetal brain. IUGR results in a regional reduction in several cell types around the ventricular and cortical regions. This interferes with producing the full complement of neurons and glia, as well as resulting in a diminution in cortical thickness with biometric microcephaly. We speculate that this early embryonic alteration in neural cellular proliferation may underlie the subsequent development of cognitive and learning disabilities during extra-uterine life seen in neonates affected by IUGR. The pro-survival effect of HN in the IUGR may underlie the increased incidence of such disabilities in the male versus the female offspring. Future investigations exploring the sex-specific function of HN in the developing brain are warranted.

Supplementary Material

Refer to Web version on PubMed Central for supplementary material.

Acknowledgements:

Confocal laser scanning microscopy was performed at the CNSI Advanced Light Microscopy/Spectroscopy Shared Resource Facility at UCLA.

Special thanks to Il Seok D. Jeong for his assistance with developing the western blot protocol for Humanin and to Jong Doo Lee, Mason Eghbali and Monique Awanyai for their technical assistance with brain tissue sectioning. We also thank Dr. Ben Novitch for helpful discussions pertaining to our Notch experiments. We are grateful to Drs. James Waschek, Pinchas Cohen and Carlos Cepeda for their guidance and helpful suggestions pertaining to this project.

Grant information: This work was supported by NIH grants HD-81206, HD-41230 (to SUD). BCS and CB were supported by the Children's Discovery and Innovation Institute United Cerebral Palsy Pilot Grant Award. CB was supported by the NIH – K12 HD34610 (to SUD), the Marshall Klaus Perinatal Research Award, and the Harry Winston Fellowship Award from the UCLA Children's Discovery and Innovation Institute.

References:

Arakawa T, Niikura T, Tajima H, & Kita Y (2006). The secondary structure analysis of a potent Ser14Gly analog of antiAlzheimer peptide, Humanin, by circular dichroism. J Pept Sci, 12(10), 639–642. doi:10.1002/psc.773 [PubMed: 16835886]

Artavanis-Tsakonas S, & Muskavitch MA (2010). Notch: the past, the present, and the future. Curr Top Dev Biol, 92, 1–29. doi:10.1016/S0070-2153(10)92001-2 [PubMed: 20816391]

Artavanis-Tsakonas S, Rand MD, & Lake RJ (1999). Notch signaling: cell fate control and signal integration in development. Science, 284(5415), 770–776. [PubMed: 10221902]

Capt C, Passamonti M, & Breton S (2016). The human mitochondrial genome may code for more than 13 proteins. Mitochondrial DNA A DNA Mapp Seq Anal, 27(5), 3098–3101. doi:10.3109/19401736.2014.1003924 [PubMed: 25630734]

Chai GS, Duan DX, Ma RH, Shen JY, Li HL, Ma ZW, … Liu G (2014). Humanin attenuates Alzheimer-like cognitive deficits and pathological changes induced by amyloid beta-peptide in rats. Neurosci Bull, 30(6), 923–935. doi:10.1007/s12264-014-1479-3 [PubMed: 25391447]

Chase HP, Welch NN, Dabiere CS, Vasan NS, & Butterfield LJ (1972). Alterations in human brain biochemistry following intrauterine growth retardation. Pediatrics, 50(3), 403–411. [PubMed: 5056413]

Chin YP, Keni J, Wan J, Mehta H, Anene F, Jia Y, … Cohen P (2013). Pharmacokinetics and tissue distribution of humanin and its analogues in male rodents. Endocrinology, 154(10), 3739–3744. doi:10.1210/en.2012-2004 [PubMed: 23836030]

Corbo JC, Deuel TA, Long JM, LaPorte P, Tsai E, Wynshaw-Boris A, & Walsh CA (2002). Doublecortin is required in mice for lamination of the hippocampus but not the neocortex. J Neurosci, 22(17), 7548–7557. [PubMed: 12196578]

Cui AL, Zhang YH, Li JZ, Song T, Liu XM, Wang H, … Li K (2017). Humanin rescues cultured rat cortical neurons from NMDA-induced toxicity through the alleviation of mitochondrial dysfunction. Drug Des Devel Ther, 11, 1243–1253. doi:10.2147/DDDT.S133042

Dahl LB, Kaaresen PI, Tunby J, Handegard BH, Kvernmo S, & Ronning JA (2006). Emotional, behavioral, social, and academic outcomes in adolescents born with very low birth weight. Pediatrics, 118(2), e449–459. doi:10.1542/peds.2005-3024 [PubMed: 16882786]

Frederiksen K, & McKay RD (1988). Proliferation and differentiation of rat neuroepithelial precursor cells in vivo. J Neurosci, 8(4), 1144–1151. [PubMed: 3357014]

Ganguly A, Collis L, & Devaskar SU (2012). Placental glucose and amino acid transport in calorie-restricted wild-type and Glut3 null heterozygous mice. Endocrinology, 153(8), 3995–4007. doi:10.1210/en.2011-1973 [PubMed: 22700768]

Ganguly A, Touma M, Thamotharan S, De Vivo DC, & Devaskar SU (2016). Maternal Calorie Restriction Causing Uteroplacental Insufficiency Differentially Affects Mammalian Placental Glucose and Leucine Transport Molecular Mechanisms. Endocrinology, 157(10), 4041–4054. doi:10.1210/en.2016-1259 [PubMed: 27494059]

Garg M, Thamotharan M, Dai Y, Lagishetty V, Matveyenko AV, Lee WN, & Devaskar SU (2013). Glucose intolerance and lipid metabolic adaptations in response to intrauterine and postnatal calorie restriction in male adult rats. Endocrinology, 154(1), 102–113. doi:10.1210/en.2012-1640 [PubMed: 23183174]

Garg M, Thamotharan M, Dai Y, Thamotharan S, Shin BC, Stout D, & Devaskar SU (2012). Early postnatal caloric restriction protects adult male intrauterine growth-restricted offspring from obesity. Diabetes, 61(6), 1391–1398. doi:10.2337/db11-1347 [PubMed: 22461568]

Garris DR (1984). Intrauterine growth of the guinea pig fetal-placental unit throughout pregnancy: regulation by utero-placental blood flow. Teratology, 29(1), 93–99. doi:10.1002/tera.1420290111 [PubMed: 6701810]

Giambrone AB, & Warrington JP (2018). The rat model of placental ischemia as a model of postpartum posterior cortical atrophy? Neural Regen Res, 13(12), 2094–2095. doi:10.4103/1673-5374.241454 [PubMed: 30323132]

Gong Z, Tasset I, Diaz A, Anguiano J, Tas E, Cui L, … Muzumdar R (2018). Humanin is an endogenous activator of chaperone-mediated autophagy. J Cell Biol, 217(2), 635–647. doi:10.1083/jcb.201606095 [PubMed: 29187525]

Gottardo MF, Jaita G, Magri ML, Zarate S, Moreno Ayala M, Ferraris J, … Seilicovich A (2014). Antiapoptotic factor humanin is expressed in normal and tumoral pituitary cells and protects them from TNF-alpha-induced apoptosis. PLoS One, 9(10), e111548. doi:10.1371/journal.pone.0111548 [PubMed: 25360890]

Hanamsagar R, & Bilbo SD (2016). Sex differences in neurodevelopmental and neurodegenerative disorders: Focus on microglial function and neuroinflammation during development. J Steroid Biochem Mol Biol, 160, 127–133. doi:10.1016/j.jsbmb.2015.09.039 [PubMed: 26435451]

Hashimoto Y, Kurita M, Aiso S, Nishimoto I, & Matsuoka M (2009). Humanin inhibits neuronal cell death by interacting with a cytokine receptor complex or complexes involving CNTF receptor alpha/WSX-1/gp130. Mol Biol Cell, 20(12), 2864–2873. doi:10.1091/mbc.E09-02-0168 [PubMed: 19386761]

Hashimoto Y, Niikura T, Tajima H, Yasukawa T, Sudo H, Ito Y, … Nishimoto I (2001). A rescue factor abolishing neuronal cell death by a wide spectrum of familial Alzheimer's disease genes and Abeta. Proc Natl Acad Sci U S A, 98(11), 6336–6341. doi:10.1073/pnas.101133498 [PubMed: 11371646]

Hernandez-Andrade E, Ahn H, Szalai G, Korzeniewski SJ, Wang B, King M, … Romero R (2014). Evaluation of utero-placental and fetal hemodynamic parameters throughout gestation in pregnant mice using high-frequency ultrasound. Ultrasound Med Biol, 40(2), 351–360. doi:10.1016/j.ultrasmedbio.2013.09.026 [PubMed: 24342911]

Howard B, Chen Y, & Zecevic N (2006). Cortical progenitor cells in the developing human telencephalon. Glia, 53(1), 57–66. doi:10.1002/glia.20259 [PubMed: 16158418]

Imamura O, Pages G, Pouyssegur J, Endo S, & Takishima K (2010). ERK1 and ERK2 are required for radial glial maintenance and cortical lamination. Genes Cells, 15(10), 1072–1088. doi:10.1111/j.1365-2443.2010.01444.x [PubMed: 20825492]

Jacobsson B, Ahlin K, Francis A, Hagberg G, Hagberg H, & Gardosi J (2008). Cerebral palsy and restricted growth status at birth: population-based case-control study. BJOG, 115(10), 1250–1255. doi:10.1111/j.1471-0528.2008.01827.x [PubMed: 18715410]

Jarvis S, Glinianaia SV, Torrioli MG, Platt MJ, Miceli M, Jouk PS, … Surveillance of Cerebral Palsy in Europe collaboration of European Cerebral Palsy, R. (2003). Cerebral palsy and intrauterine growth in single births: European collaborative study. Lancet, 362(9390), 1106–1111. doi:10.1016/S0140-6736(03)14466-2 [PubMed: 14550698]

Kariya S, Hirano M, Furiya Y, Sugie K, & Ueno S (2005). Humanin detected in skeletal muscles of MELAS patients: a possible new therapeutic agent. Acta Neuropathol, 109(4), 367–372. doi:10.1007/s00401-004-0965-5 [PubMed: 15759134]

Kim SJ, Guerrero N, Wassef G, Xiao J, Mehta HH, Cohen P, & Yen K (2016). The mitochondrial-derived peptide humanin activates the ERK1/2, AKT, and STAT3 signaling pathways and has age-dependent signaling differences in the hippocampus. Oncotarget, 7(30), 46899–46912. doi:10.18632/oncotarget.10380 [PubMed: 27384491]

Kondo S, Al-Hasani H, Hoerder-Suabedissen A, Wang WZ, & Molnar Z (2015). Secretory function in subplate neurons during cortical development. Front Neurosci, 9, 100. doi:10.3389/fnins.2015.00100 [PubMed: 25859180]

Kostyszyn B, Cowburn RF, Seiger A, Kj AA, & Sundstrom E (2001). Expression of presenilin-1 and Notch-1 receptor in human embryonic CNS. Neuroscience, 103(4), 885–898. [PubMed: 11301199]

Lavado A, & Oliver G (2011). Six3 is required for ependymal cell maturation. Development, 138(24), 5291–5300. doi:10.1242/dev.067470 [PubMed: 22071110]

Lee C, Wan J, Miyazaki B, Fang Y, Guevara-Aguirre J, Yen K, … Cohen P (2014). IGF-I regulates the age-dependent signaling peptide humanin. Aging Cell, 13(5), 958–961. doi:10.1111/acel.12243 [PubMed: 25040290]

Lee HS, Han J, Lee SH, Park JA, & Kim KW (2010). Meteorin promotes the formation of GFAP-positive glia via activation of the Jak-STAT3 pathway. J Cell Sci, 123(Pt 11), 1959–1968. doi:10.1242/jcs.063784 [PubMed: 20460434]

Leitner Y, Fattal-Valevski A, Geva R, Eshel R, Toledano-Alhadef H, Rotstein M, … Harel S (2007). Neurodevelopmental outcome of children with intrauterine growth retardation: a longitudinal, 10-year prospective study. J Child Neurol, 22(5), 580–587. doi:10.1177/0883073807302605 [PubMed: 17690065]

Li H, Chen Z, & Zhou S (2013). Apoptosis in glioma-bearing rats after neural stem cell transplantation. Neural Regen Res, 8(19), 1793–1802. doi:10.3969/j.issn.1673-5374.2013.19.007 [PubMed: 25206476]

Longo S, Bollani L, Decembrino L, Di Comite A, Angelini M, & Stronati M (2013). Short-term and long-term sequelae in intrauterine growth retardation (IUGR). J Matern Fetal Neonatal Med, 26(3), 222–225. doi:10.3109/14767058.2012.715006 [PubMed: 23030765]

Matsuoka M, Hashimoto Y, Aiso S, & Nishimoto I (2006). Humanin and colivelin: neuronal-death-suppressing peptides for Alzheimer's disease and amyotrophic lateral sclerosis. CNS Drug Rev, 12(2), 113–122. doi:10.1111/j.1527-3458.2006.00113.x [PubMed: 16958985]

Maximov V, Martynenko A, Hunsmann G, & Tarantul V (2002). Mitochondrial 16S rRNA gene encodes a functional peptide, a potential drug for Alzheimer's disease and target for cancer therapy. Med Hypotheses, 59(6), 670–673. [PubMed: 12445508]

McFarlane L, Truong V, Palmer JS, & Wilhelm D (2013). Novel PCR assay for determining the genetic sex of mice. Sex Dev, 7(4), 207–211. doi:10.1159/000348677 [PubMed: 23571295]

Men J, Zhang X, Yang Y, & Gao D (2012). An AD-related neuroprotector rescues transformed rat retinal ganglion cells from CoCl(2)-induced apoptosis. J Mol Neurosci, 47(1), 144–149. doi:10.1007/s12031-011-9701-5 [PubMed: 22222604]

Menezes JR, & Luskin MB (1994). Expression of neuron-specific tubulin defines a novel population in the proliferative layers of the developing telencephalon. J Neurosci, 14(9), 5399–5416. [PubMed: 8083744]

Middeldorp J, Boer K, Sluijs JA, De Filippis L, Encha-Razavi F, Vescovi AL, … Hol EM (2010). GFAPdelta in radial glia and subventricular zone progenitors in the developing human cortex. Development, 137(2), 313–321. doi:10.1242/dev.041632 [PubMed: 20040497]

Mizuguchi M, Qin J, Yamada M, Ikeda K, & Takashima S (1999). High expression of doublecortin and KIAA0369 protein in fetal brain suggests their specific role in neuronal migration. Am J Pathol, 155(5), 1713–1721. doi:10.1016/S0002-9440(10)65486-7 [PubMed: 10550327]

Moretti E, Giannerini V, Rossini L, Matsuoka M, Trabalzini L, & Collodel G (2010). Immunolocalization of humanin in human sperm and testis. Fertil Steril, 94(7), 2888–2890. doi:10.1016/j.fertnstert.2010.04.075 [PubMed: 20542501]

Muzumdar RH, Huffman DM, Atzmon G, Buettner C, Cobb LJ, Fishman S, … Cohen P (2009). Humanin: a novel central regulator of peripheral insulin action. PLoS One, 4(7), e6334. doi:10.1371/journal.pone.0006334 [PubMed: 19623253]

Muzumdar RH, Huffman DM, Calvert JW, Jha S, Weinberg Y, Cui L, … Lefer DJ (2010). Acute humanin therapy attenuates myocardial ischemia and reperfusion injury in mice. Arterioscler Thromb Vasc Biol, 30(10), 1940–1948. doi:10.1161/ATVBAHA.110.205997 [PubMed: 20651283]

Nikolakopoulos P, Tzimagiorgis G, Goulis DG, Chatzopoulou F, Zepiridis L, & Vavilis D (2018). Serum humanin concentrations in women with pre-eclampsia compared to women with uncomplicated pregnancies. J Matern Fetal Neonatal Med, 31(3), 305–311. doi:10.1080/14767058.2017.1285885 [PubMed: 28110609]

Padilla N, Falcon C, Sanz-Cortes M, Figueras F, Bargallo N, Crispi F, … Gratacos E (2011). Differential effects of intrauterine growth restriction on brain structure and development in preterm infants: a magnetic resonance imaging study. Brain Res, 1382, 98–108. doi:10.1016/j.brainres.2011.01.032 [PubMed: 21255560]

Pryor J, Silva PA, & Brooke M (1995). Growth, development and behaviour in adolescents born small-for-gestational-age. J Paediatr Child Health, 31(5), 403–407. [PubMed: 8554859]

Raikkonen K, Pesonen AK, Heinonen K, Kajantie E, Hovi P, Jarvenpaa AL, … Andersson S (2008). Depression in young adults with very low birth weight: the Helsinki study of very low-birth-weight adults. Arch Gen Psychiatry, 65(3), 290–296. doi:10.1001/archgenpsychiatry.2007.40 [PubMed: 18316675]

Resnik R (2002). Intrauterine growth restriction. Obstet Gynecol, 99(3), 490–496. [PubMed: 11864679]

Robertson CM, Etches PC, & Kyle JM (1990). Eight-year school performance and growth of preterm, small for gestational age infants: a comparative study with subjects matched for birth weight or for gestational age. J Pediatr, 116(1), 19–26. [PubMed: 2295960]

Samuelsen GB, Pakkenberg B, Bogdanovic N, Gundersen HJ, Larsen JF, Graem N, & Laursen H (2007). Severe cell reduction in the future brain cortex in human growth-restricted fetuses and infants. Am J Obstet Gynecol, 197(1), 56 e51–57. doi:10.1016/j.ajog.2007.02.011 [PubMed: 17618757]

Schambra U (2008). PRENATAL MOUSE BRAIN ATLAS (Atlas). Available from Springer Science +Business Media, LLC (978-0-387-47089-4). https://link.springer.com/content/pdf/10.1007%2F978-0-387-47093-1.pdf

Schwarz JM, & Bilbo SD (2012). Sex, glia, and development: interactions in health and disease. Horm Behav, 62(3), 243–253. doi:10.1016/j.yhbeh.2012.02.018 [PubMed: 22387107]

Schwarz JM, Sholar PW, & Bilbo SD (2012). Sex differences in microglial colonization of the developing rat brain. J Neurochem, 120(6), 948–963. doi:10.1111/j.1471-4159.2011.07630.x [PubMed: 22182318]

Sherry MM, Reeves A, Wu JK, & Cochran BH (2009). STAT3 is required for proliferation and maintenance of multipotency in glioblastoma stem cells. Stem Cells, 27(10), 2383–2392. doi:10.1002/stem.185 [PubMed: 19658181]

Shin BC, Suzuki T, Tanaka S, Kuraoka A, Shibata Y, & Takata K (1996). Connexin 43 and the glucose transporter, GLUT1, in the ciliary body of the rat. Histochem Cell Biol, 106(2), 209–214. [PubMed: 8877381]

Smedler AC, Faxelius G, Bremme K, & Lagerstrom M (1992). Psychological development in children born with very low birth weight after severe intrauterine growth retardation: a 10-year follow-up study. Acta Paediatr, 81(3), 197–203. [PubMed: 1511191]

Sommer I, & Schachner M (1981). Monoclonal antibodies (O1 to O4) to oligodendrocyte cell surfaces: an immunocytological study in the central nervous system. Dev Biol, 83(2), 311–327. [PubMed: 6786942]

Sreekumar PG, Ishikawa K, Spee C, Mehta HH, Wan J, Yen K, … Hinton DR (2016). The Mitochondrial-Derived Peptide Humanin Protects RPE Cells From Oxidative Stress, Senescence, and Mitochondrial Dysfunction. Invest Ophthalmol Vis Sci, 57(3), 1238–1253. doi:10.1167/iovs.15-17053 [PubMed: 26990160]

Strauss RS (2000). Adult functional outcome of those born small for gestational age: twenty-six-year follow-up of the 1970 British Birth Cohort. JAMA, 283(5), 625–632. [PubMed: 10665702]

Tajima H, Niikura T, Hashimoto Y, Ito Y, Kita Y, Terashita K, … Nishimoto I (2002). Evidence for in vivo production of Humanin peptide, a neuroprotective factor against Alzheimer's disease-related insults. Neurosci Lett, 324(3), 227–231. [PubMed: 12009529]

Terashita K, Hashimoto Y, Niikura T, Tajima H, Yamagishi Y, Ishizaka M, … Nishimoto I (2003). Two serine residues distinctly regulate the rescue function of Humanin, an inhibiting factor of Alzheimer's disease-related neurotoxicity: functional potentiation by isomerization and dimerization. J Neurochem, 85(6), 1521–1538. [PubMed: 12787071]

Tolcos M, Markwick R, O'Dowd R, Martin V, Turnley A, & Rees S (2015). Intrauterine Growth Restriction: Effects on Neural Precursor Cell Proliferation and Angiogenesis in the Foetal Subventricular Zone. Dev Neurosci, 37(4-5), 453–463. doi:10.1159/000371344 [PubMed: 25720426]

Tolsa CB, Zimine S, Warfield SK, Freschi M, Sancho Rossignol A, Lazeyras F, … Huppi PS (2004). Early alteration of structural and functional brain development in premature infants born with intrauterine growth restriction. Pediatr Res, 56(1), 132–138. doi:10.1203/01.PDR.0000128983.54614.7E [PubMed: 15128927]

Tomi M, Zhao Y, Thamotharan S, Shin BC, & Devaskar SU (2013). Early life nutrient restriction impairs blood-brain metabolic profile and neurobehavior predisposing to Alzheimer's disease with aging. Brain Res, 1495, 61–75. doi:10.1016/j.brainres.2012.11.050 [PubMed: 23228723]

Tomioka M, Nishimoto M, Miyagi S, Katayanagi T, Fukui N, Niwa H, … Okuda A (2002). Identification of Sox-2 regulatory region which is under the control of Oct-3/4-Sox-2 complex. Nucleic Acids Res, 30(14), 3202–3213. [PubMed: 12136102]

Tserentsoodol N, Shin BC, Koyama H, Suzuki T, & Takata K (1999). Immunolocalization of tight junction proteins, occludin and ZO-1, and glucose transporter GLUT1 in the cells of the blood-nerve barrier. Arch Histol Cytol, 62(5), 459–469. [PubMed: 10678575]

Vandenbosche RC, & Kirchner JT (1998). Intrauterine growth retardation. Am Fam Physician, 58(6), 1384–1390, 1393-1384. [PubMed: 9803202]

Wang S, Chandler-Militello D, Lu G, Roy NS, Zielke A, Auvergne R, … Goldman SA (2010). Prospective identification, isolation, and profiling of a telomerase-expressing subpopulation of human neural stem cells, using sox2 enhancer-directed fluorescence-activated cell sorting. J Neurosci, 30(44), 14635–14648. doi:10.1523/JNEUROSCI.1729-10.2010 [PubMed: 21048121]

Wang T, Yuan W, Liu Y, Zhang Y, Wang Z, Zhou X, … Kong X (2015). The role of the JAK-STAT pathway in neural stem cells, neural progenitor cells and reactive astrocytes after spinal cord injury. Biomed Rep, 3(2), 141–146. doi:10.3892/br.2014.401 [PubMed: 25798237]

Widmer RJ, Flammer AJ, Herrmann J, Rodriguez-Porcel M, Wan J, Cohen P, … Lerman A (2013). Circulating humanin levels are associated with preserved coronary endothelial function. Am J Physiol Heart Circ Physiol, 304(3), H393–397. doi:10.1152/ajpheart.00765.2012 [PubMed: 23220334]

Windrem MS, Nunes MC, Rashbaum WK, Schwartz TH, Goodman RA, McKhann G 2nd, … Goldman SA (2004). Fetal and adult human oligodendrocyte progenitor cell isolates myelinate the

congenitally dysmyelinated brain. Nat Med, 10(1), 93–97. doi:10.1038/nm974 [PubMed: 14702638]

Wnuk A, Rzemieniec J, Litwa E, Lason W, & Kajta M (2018). Prenatal exposure to benzophenone-3 (BP-3) induces apoptosis, disrupts estrogen receptor expression and alters the epigenetic status of mouse neurons. J Steroid Biochem Mol Biol, 182, 106–118. doi:10.1016/j.jsbmb.2018.04.016 [PubMed: 29704544]

Xiao D, & Zhang L (2008). Upregulation of Bax and Bcl-2 following prenatal cocaine exposure induces apoptosis in fetal rat brain. Int J Med Sci, 5(6), 295–302. [PubMed: 18974856]

Xu X, Chua CC, Gao J, Hamdy RC, & Chua BH (2006). Humanin is a novel neuroprotective agent against stroke. Stroke, 37(10), 2613–2619. doi:10.1161/01.STR.0000242772.94277.1f [PubMed: 16960089]

Ying G, Iribarren P, Zhou Y, Gong W, Zhang N, Yu ZX, … Wang JM (2004). Humanin, a newly identified neuroprotective factor, uses the G protein-coupled formylpeptide receptor-like-1 as a functional receptor. J Immunol, 172(11), 7078–7085. [PubMed: 15153530]

Yoshimatsu T, Kawaguchi D, Oishi K, Takeda K, Akira S, Masuyama N, & Gotoh Y (2006). Non-cell-autonomous action of STAT3 in maintenance of neural precursor cells in the mouse neocortex. Development, 133(13), 2553–2563. doi:10.1242/dev.02419 [PubMed: 16728475]

Zecevic N (2004). Specific characteristic of radial glia in the human fetal telencephalon. Glia, 48(1), 27–35. doi:10.1002/glia.20044 [PubMed: 15326612]

Zhao J, Wang D, Li L, Zhao W, & Zhang C (2014). Protective effects of humanin on okadaic Acid-induced neurotoxicities in cultured cortical neurons. Neurochem Res, 39(11), 2150–2159. doi:10.1007/s11064-014-1410-3 [PubMed: 25142935]

Zubrick SR, Kurinczuk JJ, McDermott BM, McKelvey RS, Silburn SR, & Davies LC (2000). Fetal growth and subsequent mental health problems in children aged 4 to 13 years. Dev Med Child Neurol, 42(1), 14–20. [PubMed: 10665970]

Significance Statement

The intrauterine environment has tremendous potential to shape extra-uterine life. Maternal malnutrition detrimentally affects brain development in utero leading to life-long adverse neurological consequences. Our study has unraveled perturbations caused by maternal caloric restriction on the embryonic brain cellular profile which may contribute to the ultimate structural and functional abnormalities of the intra-uterine growth restricted (IUGR) offspring. Additionally, this study is the first to examine an endogenous neuroprotective peptide, Humanin, during fetal life. Exploration of cellular and structural brain abnormalities resulting from IUGR contributes to the search for mechanisms to promote healthy neurodevelopment.

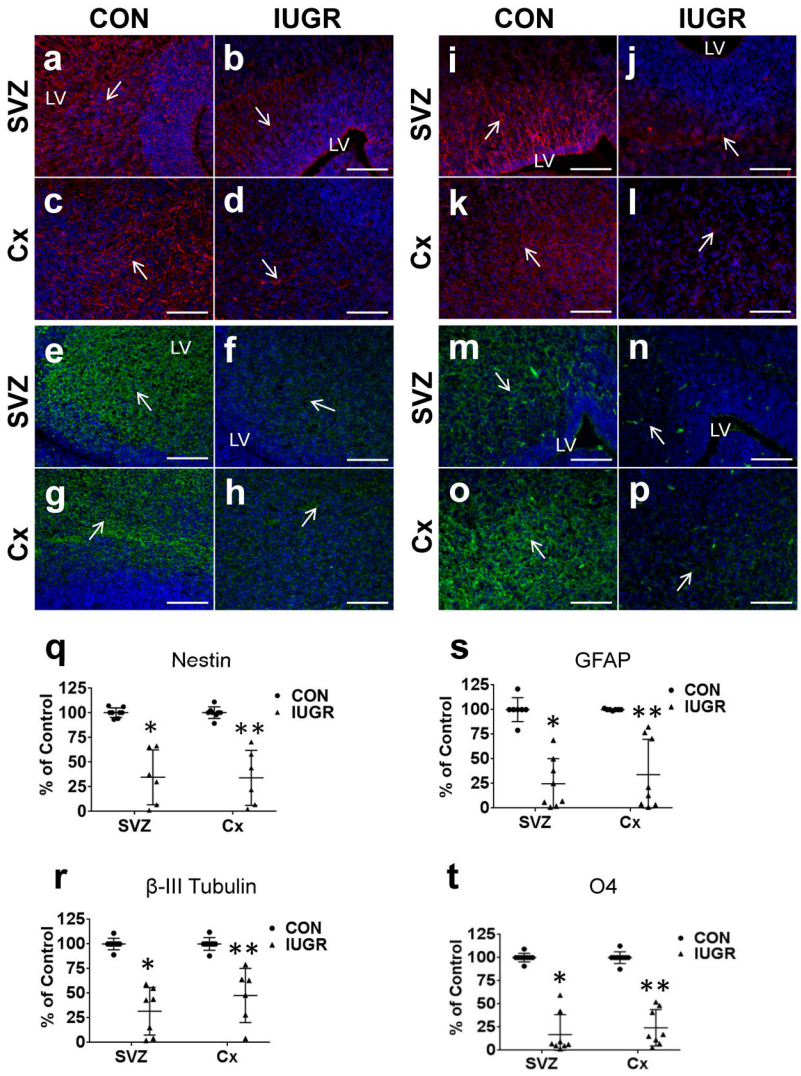

Figure 1.

Comparison of cellular profile within intra-uterine growth restricted (IUGR) versus control murine fetal brain in regions of the subventricular zone (SVZ) and cerebral cortex (Cx). 10 μM coronal frozen sections were taken at embryonic day 19. Fluorescence quantification of IUGR versus control were compared using two-tailed Student t-test. Male and female samples were pooled. The IUGR brain demonstrated significantly lower expression than control in all markers (nestin, β-III Tubulin, GFAP, O4). ***a-d***, nestin (red) expression, a cytoskeletal protein marking neural progenitor cells (arrows). ***q***, Nestin quantification (CON n=8, IUGR n=6) in SVZ (t_5 = 5.69; **P*=0.002) and Cx (t_5 = 5.71; ***P*=0.002). ***e-h***, β-III Tubulin expression (green), marking newly generated immature neurons (arrows). ***r***, β-III Tubulin quantification (CON n=8, IUGR n=7) in SVZ (t_6 = 7.31; **P*<0.001) and Cx: (t_6 = 4.58; ***P*=0.004). ***i-l,*** Glial fibrillary acidic protein (GFAP) (red), a marker for astrocytes (arrows). ***s,*** GFAP quantification (n=7/group) in SVZ (t_8 = 6.59; **P*<0.001) and Cx (t_6 = 5.2; ***P*=0.002). ***m-p***, O4 (green), a marker for mature, immature, and pre-oligodendrocytes (arrows). ***t***, O4 quantification (CON n=9, IUGR n=8) in SVZ (t_7 = 10.73; **P*<0.001) and Cx

(t_8 = 10.51; **P<0.001). Fluorescence quantification is shown (***q*-*t***) with IUGR expressed as a percent of control. Data are shown as means ± standard deviation. Scale bars 100 μM.

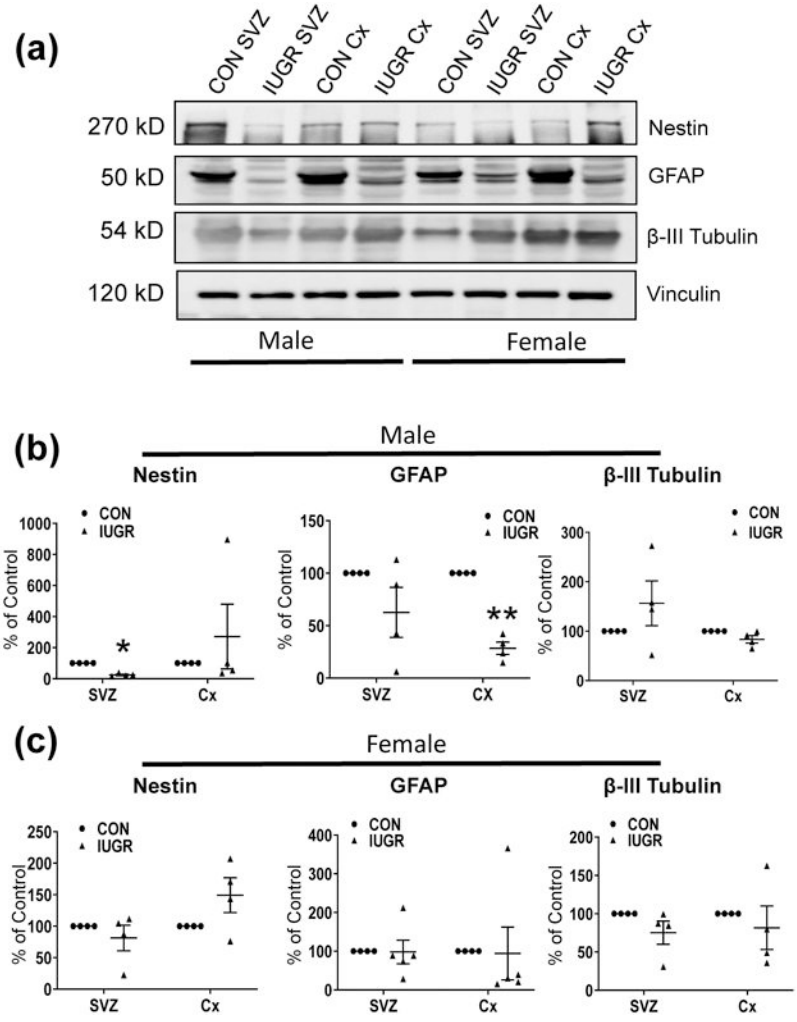

Figure 2.

Western blot analysis examining murine fetal brain in regions of the subventricular zone (SVZ) and cerebral cortex (Cx) lysate of males and females at embryonic day 19 in control versus intra-uterine growth restricted (IUGR) fetal mice. ***a***, Representative western blots demonstrating nestin, Glial Fibrillary Acidic Protein (GFAP) and β-III Tubulin on the top with their corresponding loading controls (Vinculin) below. N=4/group. ***b, c*** Graphs demonstrating the quantification of protein density as a ratio to the loading control, expressed as a percent of control in males (***b***) and females (***c***) respectively. Using two-tailed Student t-test, IUGR and CON groups were compared in SVZ and Cx regions for both sexes. Significant difference was found for nestin in the male SVZ and GFAP in the male Cx (nestin: t_6=15.77, *P<0.0001; GFAP: t_6=12.08, **P<0.0001). The remaining comparisons were not significant. N=4/group, data are shown as means ± standard error of the mean.

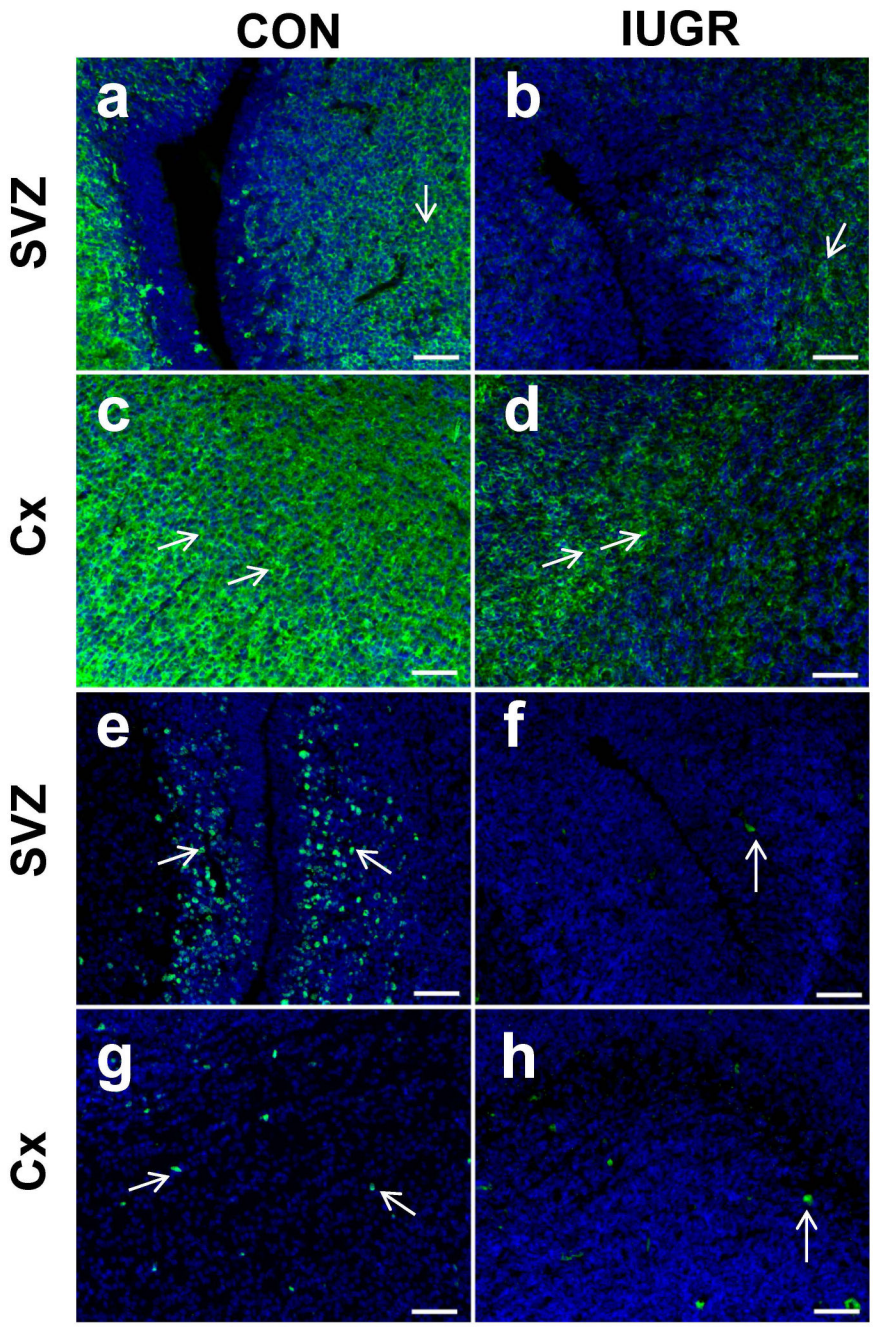

Figure 3.

Comparison of doublecortin (***a-d***) and Ki67 (***e-h***) expression within control versus intra-uterine growth restricted (IUGR) murine fetal brain in regions of the subventricular zone (SVZ) and cerebral cortex (Cx). 10 μM coronal frozen sections taken at embryonic day 19. Doublecortin is a marker for neural migration, and Ki67 is a marker for proliferation. There appears to be qualitatively a lower expression in the IUGR brain for both markers. Scale bars 50 μM.

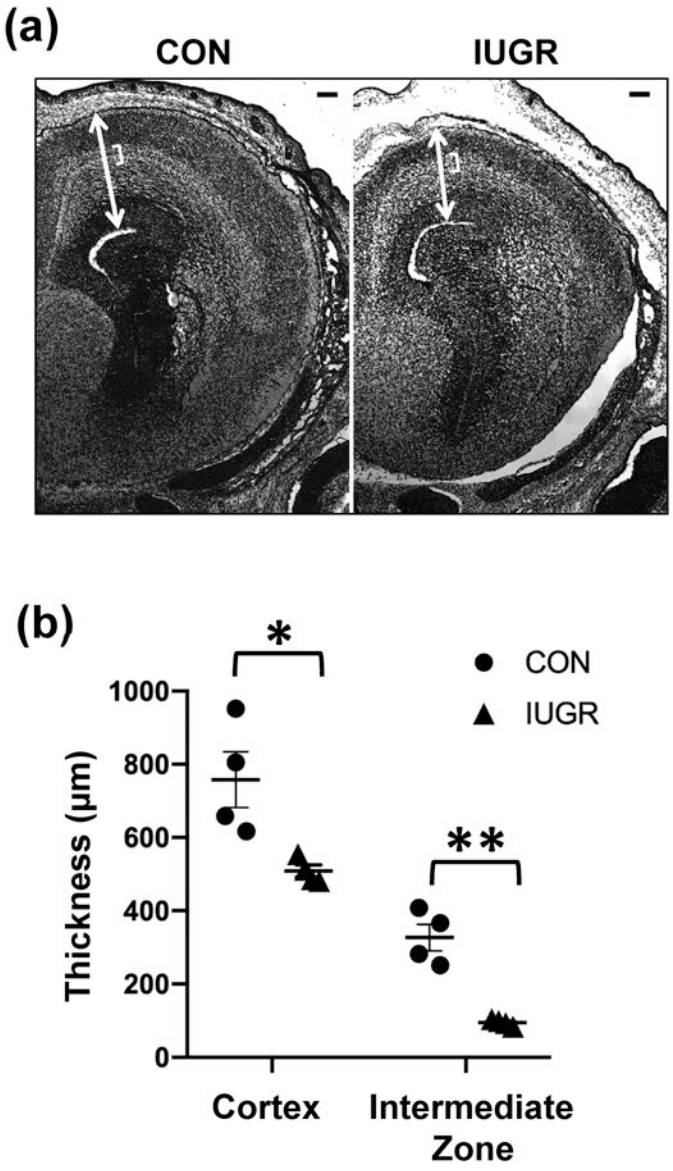

Figure 4.

Cortical thickness of control versus intra-uterine growth restricted (IUGR) fetal murine brain at embryonic day 19. Sections were 10 μM frozen coronal with pooled male and female samples. ***a***, Full cerebral cortex thickness was measured from the edge of the lateral ventricle through the marginal zone in a perpendicular orientation to the cortical layers (depicted by a large white arrow). Intermediate zone thickness was measured from the edge of the cortical plate to the edge of the subventricular zone (red bracket) ***b,*** Quantification using two-tailed Student t-test (n=4/group) showed a 29.5% reduction in cerebral cortex thickness of the IUGR brain compared to control (t_6 =2.8, **P*-value=0.031). There was a 71% reduction in intermediate zone thickness of the IUGR brain compared to control (t_6=6.3, ***P*-value=0.0007). Scale bars 50 μM. Data are shown as means ± standard deviation.

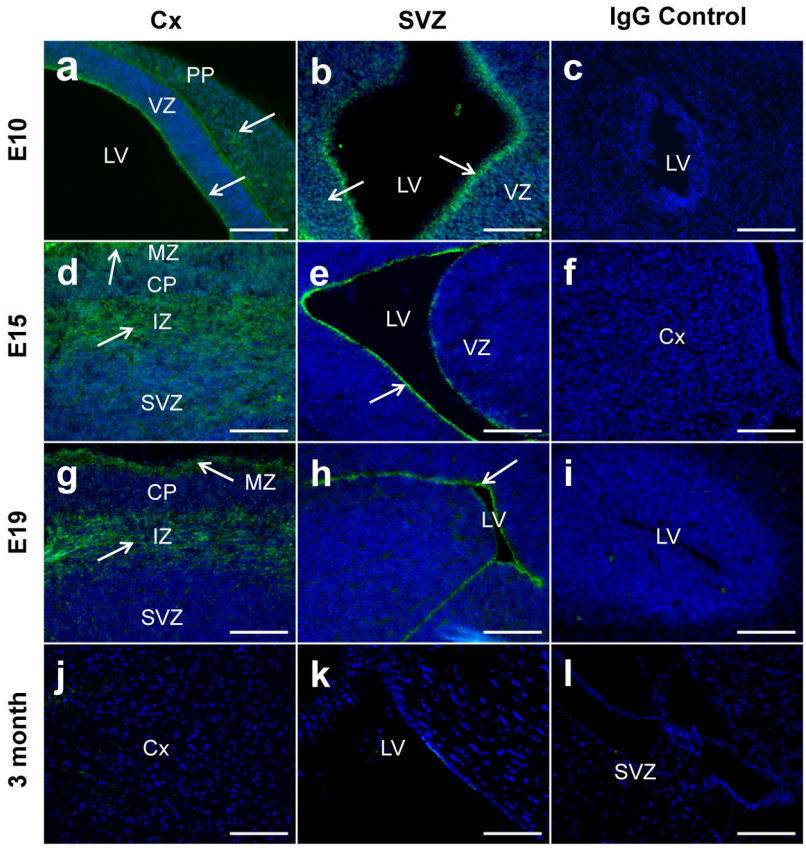

Figure 5.

Immunofluorescence staining of mouse Humanin (mHN) expression (green) in the cerebral cortex (Cx) and subventricular zone (SVZ) at differing stages of murine brain development. Sections were frozen 10 μM and coronal. ***a-c***, At embryonic day (E10) the cortex has only two layers, the ventricular zone (VZ) and pre-plate (PP) with both expressing mHN (arrows). ***d-f***, At E15 mHN was expressed strongly in the marginal zone (MZ) and intermediate zone (IZ) of the Cx (arrows) with lighter staining within the cortical plate (CP). Periventricular cells lining the lateral ventricle (LV) also show mHN expression (arrow). ***g-i,*** Similar to E15 Cx, mHN expression at E19 was localized to the MZ and IZ of the Cx as well as periventricular cells (arrows). By the adult stage at 3 months ***(j-l)***, mHN was minimally expressed. Scale bars, 100 μm.

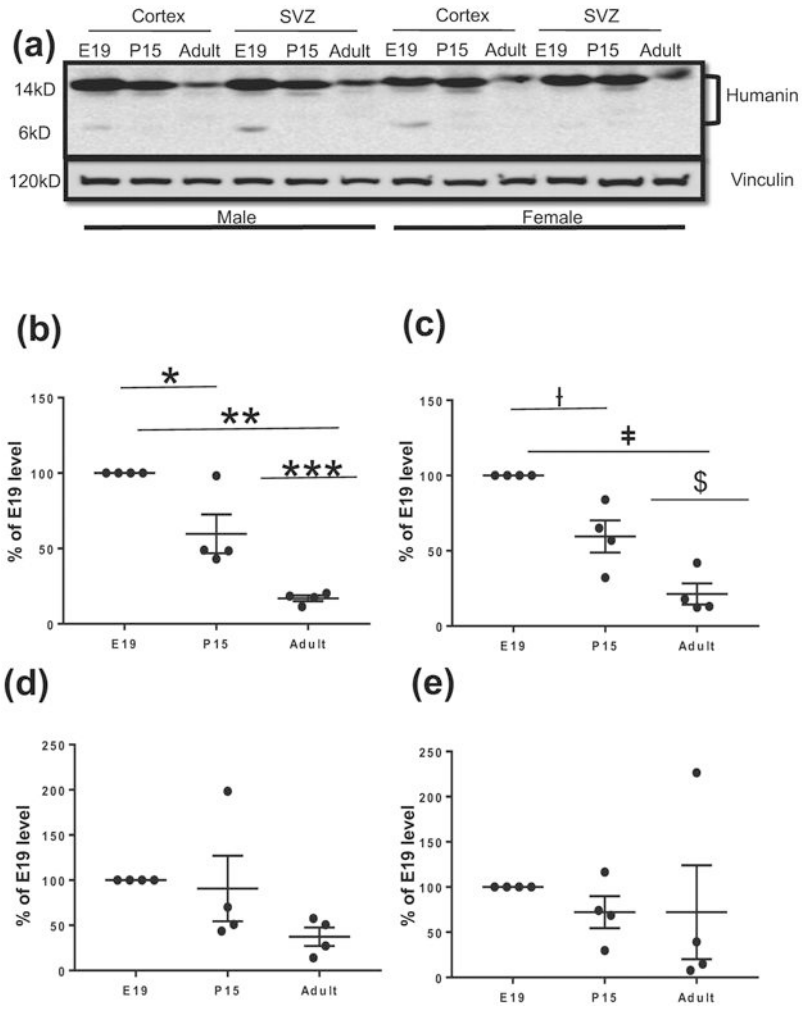

Figure 6.

Western blot analysis demonstrating mouse Humanin (mHN) expression in regions of the subventricular zone (SVZ) and cerebral cortex (Cx) at three developmental time points in males and females (n=4/group): embryonic day 19 (E19), post-natal day 15 (P15) and 3-month-old adult. ***a,*** Representative Western blots for males (left) and females (right) probed with anti-HN antibody. Corresponding vinculin loading control shown below. Both 14kD and 6kD bands were included in the quantification for mHN. Multiple comparison of mHN expression in males (***b, c)*** and females ***(d,e)*** in the Cx and SVZ regions at the three developmental time points. Quantification of protein density given as a ratio to vinculin, expressed as a percent of E19 concentration. One-way ANOVA with Fisher's PLSD was performed and there were significant differences between groups in males, but not females. Expression of mHN decreased over time with highest amounts at E19 and lowest in adulthood. In the male Cx: *F(2, 9)=30.53*, P<0.0001, *P=0.004, *P<0.001 and ***P=0.003; in male SVZ, *F(2, 9)=28.38* ǂP=0.004,ǂP<0.001, $P=0.005; Females appeared to trend in this pattern as well but the results did not reach significance. NS, non-significant. Data are shown as means ± standard error of the mean.

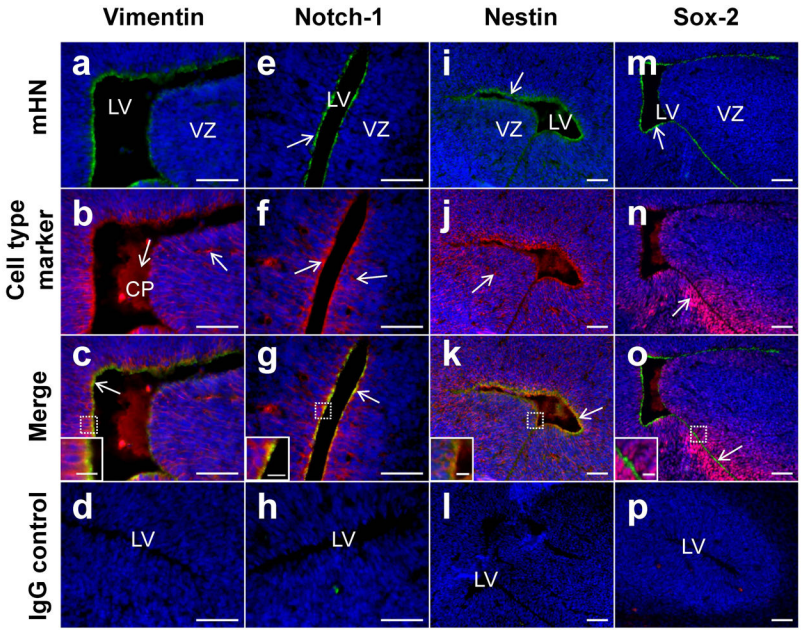

Figure 7.

Dual immunostaining of mouse Humanin (mHN) (green, first row) plus each of four different cell markers with known periventricular expression (red, second row). DAPI is blue. Coronal frozen sections at 10 μM of murine brain at embryonic day 19 (E19) in the region of the ventricular zone (VZ). White dotted boxes in the merged images outline an area focused upon to increase magnification in order to present details in an inset at the bottom left corner of the image. Expression of mHN in this area was within the periventricular cells lining the lateral ventricle (LV) (see arrows). ***a-d***, Vimentin is an intermediate filament protein expressed in mesenchymal cells and several neural cell types. Here its expression as seen in the choroid plexus (CP), periventricular cells, and throughout the VZ (arrows at CP and VZ). Merged image reveals discrete red and green signals indicating that Vimentin and mHN co-express in some cells but do not co-localize (arrow). ***e-h,*** Notch-1 is a transmembrane signaling protein that helps maintain radial glial cells (RGCs) in their undifferentiated state. Notch-1 demonstrates expression in the periventricular cells extending to the VZ (one arrow each site). Merged images appear yellow at the ventricular surface (arrow), however confocal imaging (Supplemental Video 2*)* demonstrates no true co-localization. ***i-l,*** Nestin is an intermediate filament protein expressed in progenitor cells during the early stages of central nervous system development. Nestin was seen throughout the VZ (arrow) with some cells expressing both nestin and mHN, though no co-localization was seen (arrow). ***m-p,*** Sox-2 is a transcription factor essential for maintaining pluripotency of embryonic stem cells. Sox-2 staining was seen in the nucleus, appearing pink where it co-expresses with DAPI (arrow in VZ demonstrating pink cells). Expression was strongest in the VZ, decreasing as it moves away from the LV. Clear separation of red and green signals indicated no co-localization between mHN and Sox-2 (arrow). Scale bars, 50 μm. Inset image (in merged images) scale bars = 10 μm.

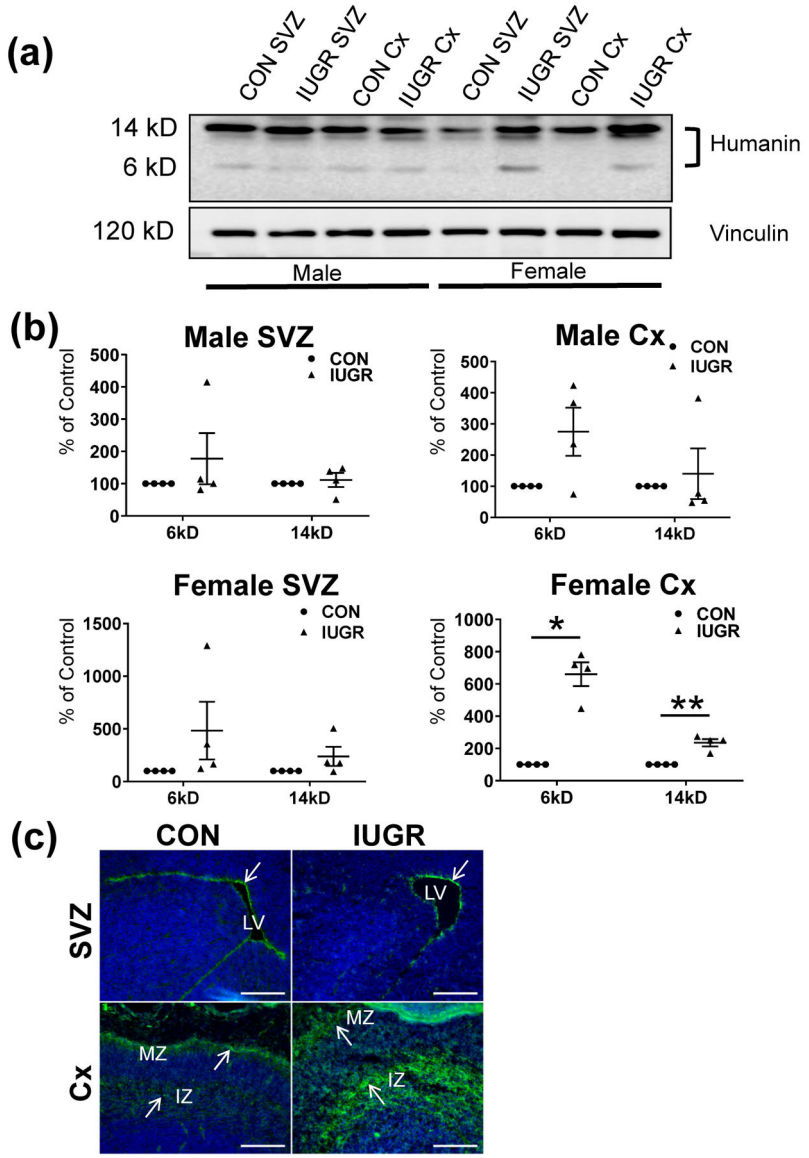

Figure 8.

Western blots (***a*** **&** ***b***) and immunostaining (***c***) of mouse Humanin (mHN) protein, in control versus intra-uterine growth restricted (IUGR) murine embryonic day 19 (E19) fetal brain in regions of the subventricular zone (SVZ) and cerebral cortex (Cx). ***a***, Representative western blots showing both 14kD and 6kD mHN bands in males (left lanes) and females (right lanes). ***b,*** Quantification of mHN protein density as a ratio to loading control, expressed as a percent of control. Results were analyzed as sex-specific sub-sets, region specific (SVZ and Cx) and protein bands (14kD and 6kD) as labeled. In female Cx, both mHN at 6kD and 14kD were significantly increased in IUGR compared with CON (6kD, t_6=7.7611, *p=0.0003; 14kD, t_6=5.913, **p=0.001). Statistical test was two-tailed Student t-test with n=4/group, Data are shown as means ± standard error of the mean. ***c***, Immunostaining of mHN coronal frozen sections (10 μM) taken at embryonic day 19 (E19). Control and IUGR brain demonstrate similar expression patterns. Within the SVZ, mHN was expressed in

periventricular cells lining the lateral ventricle (LV) while in the Cx it was primarily within the intermediate zone (IZ) and marginal zone (MZ) (arrows). Scale bars 100μM.

Table 1.

Antibody details and concentration

Name (detects)	Immunogen structure	Manufacturer details	Concentration/Data type
Humanin (mouse Humanin)	Humanin protein residues 9-24	Sigma-Aldrich Cat No: H2414 RRID:AB_532250 Species: Rabbit Polyclonal	1:300/ Western blot; IHC
Nestin (neural progenitors)	Recombinant rat Nestin (rrNestin; aa 544 - 776)	Neuromics Cat No: GT15114 RRID:AB_1619688 Species: Goat Polyclonal	1:2000/ Western blot 1:100/ IHC
Glial Fibrillary Acidic Protein (astrocytes)	Recombinant GFAP and purified bovine GFAP	Neuromics Cat No: RA22101 RRID:AB_1616567 Species: Rabbit Polyclonal	1:1000/ Western blot; IHC
β-III Tubulin (immature neurons)	Microtubules derived from rat brain; highly reactive to neuron specific Class III	Covance (Now BioLegend) Cat No: MMS-425P RRID:AB_2313773 Species: Mouse Monoclonal	1:8000/ Western blot 1:200/ IHC
Vimentin (mesenchymal cells, radial glial cells)	Epitope mapping at the C-terminus of Vimentin of human origin	Santa Cruz Biotechnologies Cat No: sc-7557 RRID:AB_793998 Species: Goat Polyclonal	1:1200/ IHC
Notch-1 (cell fate signaling)	Epitope mapping at the C-terminus of Notch 1 of human origin	Santa Cruz Biotechnologies Cat No: sc-6014 RRID:AB_650336 Species: Goat Polyclonal	1:200/ IHC
Sox-2 (stem cells)	Epitope mapping near the C-terminus of Sox-2 of human origin	Santa Cruz Biotechnologies Cat No: sc-17320 RRID:AB_2286684 Species: Goat Polyclonal	1:2000/ IHC
O4 (mature, immature, and pre-oligodendrocytes, myelin)	White matter of corpus callosum from bovine brain	Sigma-Aldrich Cat No: O7139 RRID:AB_477662 Species: Mouse Monoclonal	1:50/ IHC
Bcl-2 (Anti-apoptosis)	Synthetic peptide corresponding to Bcl-2 aa 41-54	Abcam Cat No: ab692 RRID:AB_305670 Species: Mouse Monoclonal	1:500/ Western blot
Bax (Pro-apoptosis)	A synthetic peptide corresponding to the amino-terminal residues of human Bax	Cell Signaling Technology Cat No: 2772 RRID:AB 10695870 Species: Rabbit Polyclonal	1:500/ Western blot
B-Actin	A synthetic peptide corresponding to residues near the amino terminus of human β-actin protein.	Cell Signaling Technology, Cat No: 8457 RRID: AB_10950489 Species: Rabbit Monoclonal	1:20,000/Western blot
Vinculin	Derived from the hVIN-1 hybridoma produced by the fusion of mouse myeloma cells and splenocytes from immunized BALB/c mice.	Sigma-Aldrich Cat No: V9131 RRID: AB_477629	1:60,000/Western blot

Name (detects)	Immunogen structure	Manufacturer details	Concentration/Data type
		Species: Mouse Monoclonal	
GAPDH	A synthetic peptide near the carboxy terminus of human GAPDH.	Cell Signaling Technology, Cat No: 2118 RRID: AB_561053 Species: Rabbit Monoclonal	1:20,000/Western blot
Ki67 (proliferation)	Synthetic peptide conjugated to KLH derived from within residues 1200 - 1300 of Human Ki67.	Abcam Cat No: ab15580 RRID:AB_443209 Species: Rabbit Polyclonal	1:500/ IHC
Doublecortin (neural migration)	Synthetic peptide conjugated to KLH derived from within residues 300 to the C-terminus of Human Doublecortin	Abcam Cat No: ab18723, RRID:AB_732011 Species: Rabbit Polyclonal	1:1000/ IHC